

NASA-TM-83525

NASA Technical Memorandum 83525

NASA-TM-83525 19840005856

Inverted Velocity Profile Semi-Annular Nozzle Jet Exhaust Noise Experiments

Jack H. Goodykoontz
Lewis Research Center
Cleveland, Ohio

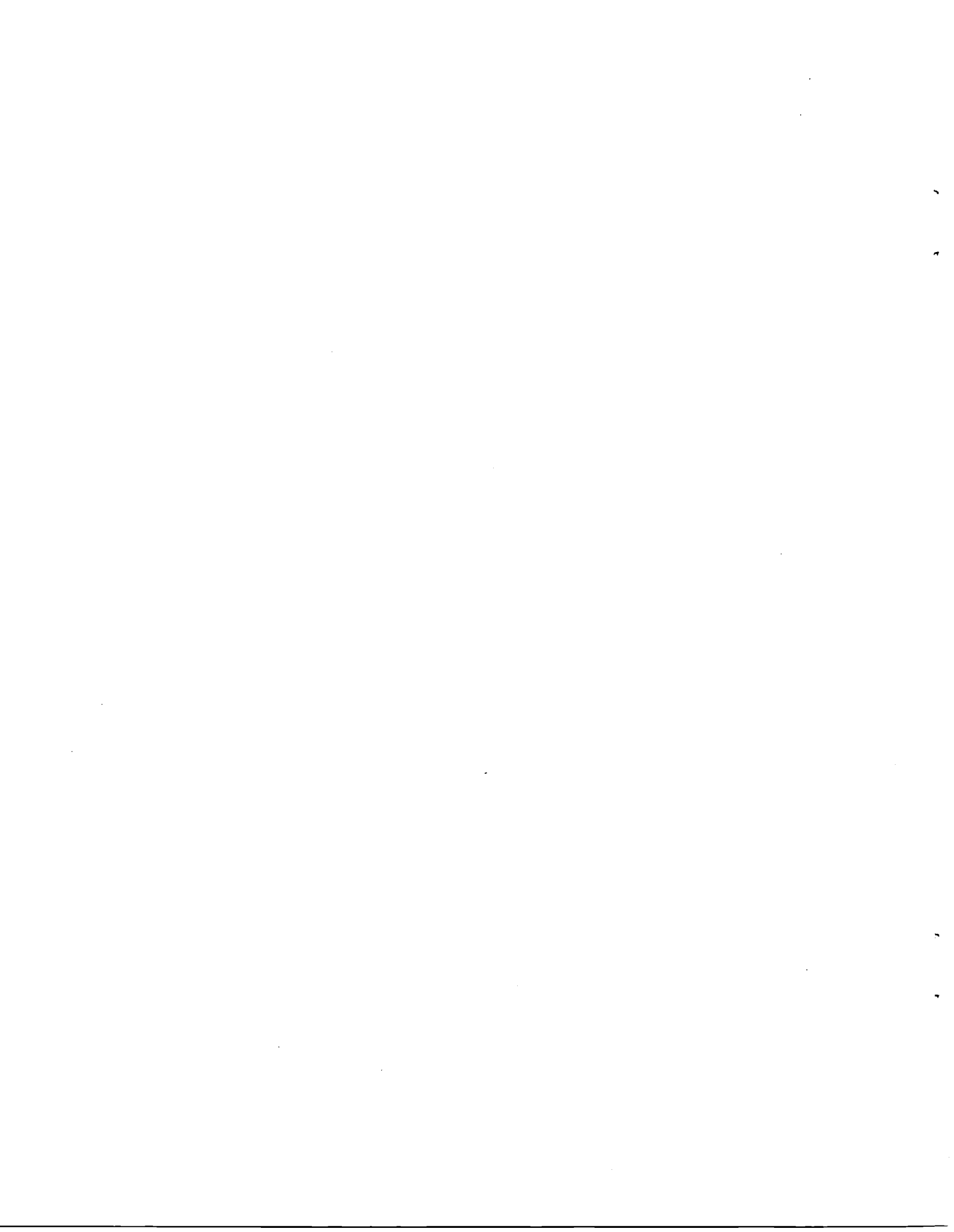
December 1983

LIBRARY COPY

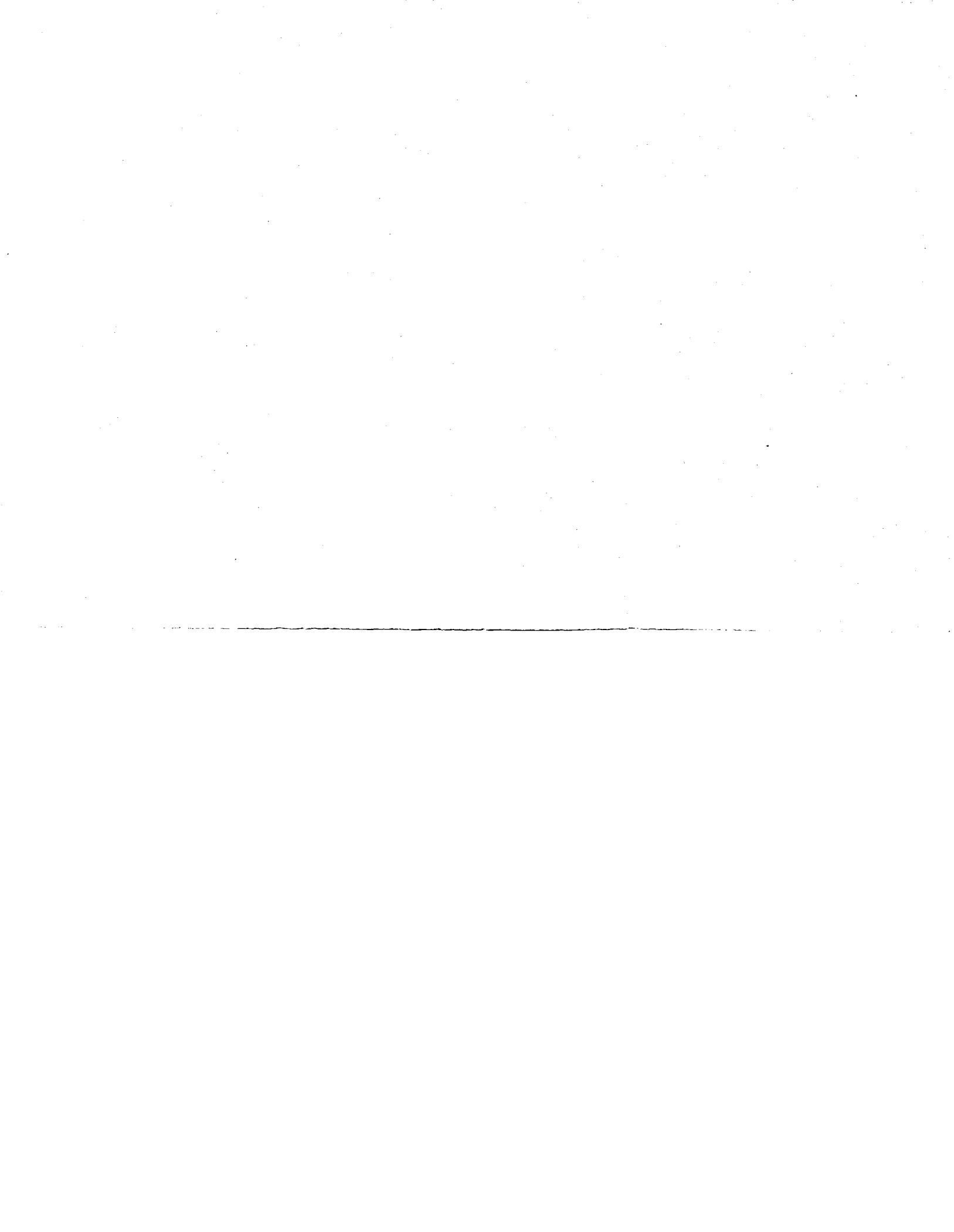
JUN 23 1984

LANGLEY RESEARCH CENTER
LIBRARY, NASA
HAMPTON, VIRGINIA

NASA



46 1 1 RN/NASA-TM-83525
DISPLAY 46/2/1
84M13924** ISSUE 4 PAGE 595 CATEGORY 71 RPT#: NASA-TM-83525 E-1890
NAS 1.15:83525 83/12/00 23 PAGES UNCLASSIFIED DOCUMENT
UTTL: Inverted velocity profile semi-annular nozzle jet exhaust noise
experiments
AUTH: A/GOODYKOONTZ, J. H.
CORP: National Aeronautics and Space Administration, Lewis Research Center,
Cleveland, Ohio. AVAIL NTIS SAP: HC A02/MF A01
MAJS: /*ANNULAR NOZZLES/*CONICAL NOZZLES/*EXHAUST NOZZLES/*JET AIRCRAFT NOISE/*
NOISE REDUCTION/*NOISE SPECTRA
MINS: / EFFECTIVE PERCEIVED NOISE LEVELS/ FLOW VELOCITY/ MULTIPHASE FLOW/ NOZZLE
FLOW/ SECONDARY FLOW
ABA: Author
ABS: Experimental noise data are shown for a conical nozzle with a semi-annular
secondary flow passage having secondary to primary velocity ratios ranging
from 1.0 to 1.4. Spectral data are presented at different directivity
angles in the flyover plane with the semi-annular flow passage located
either on the same side or opposite side relative to an observer. A 10.0
cm diameter primary conical nozzle was used with a 2.59 cm and 5.07 cm
wide annular gap secondary nozzle. Similar trends were observed for both
nozzle configurations. In general, near the peak noise location and at
velocity ratios greater than 1.0, noise levels were larger on the side
where the secondary passage was closest to an observer. At velocity ratios
ENTER:



INVERTED VELOCITY PROFILE SEMI-ANNULAR NOZZLE
JET EXHAUST NOISE EXPERIMENTS

Jack H. Goodykoontz

National Aeronautics and Space Administration
Lewis Research Center
Cleveland, Ohio 44135

SUMMARY

E-1890

Experimental noise data are shown for a conical nozzle with a semi-annular secondary flow passage having secondary to primary velocity ratios ranging from 1.0 to 1.4. Spectral data are presented at different directivity angles in the flyover plane with the semi-annular flow passage located either on the same side or opposite side relative to an observer. A 10.0 cm diameter primary conical nozzle was used with a 2.59 and 5.07 cm wide annular gap secondary nozzle. Similar trends were observed for both nozzle configurations. In general, near the peak noise location and at velocity ratios greater than 1.0, noise levels were larger on the side where the secondary passage was closest to an observer. At velocity ratios near 1.0 the opposite was true. When compared to predicted noise levels for a conical nozzle alone operating at the same ideal thrust, the semi-annular configuration showed no benefit in terms of noise attenuation.

INTRODUCTION

This report presents additional results from an experimental program that was designed to investigate methods for the attenuation of jet exhaust noise. The experimental work consisted of two phases. The first phase (refs. 1 and 2) investigated the attenuating effects of a thermal acoustic shield (TAS) configuration, where a high temperature, low-velocity, semi-annular gas stream flowed adjacent to the main propulsion stream from a primary conical nozzle. The results of the first phase of this program showed that a sizeable decrease in high frequency noise was attained with the TAS configuration. However, the configuration was handicapped since thrust loss (possibly prohibitive) was inherent in the design (assuming that, for a practical application, the shield stream was bled from the main propulsion stream with shield to primary velocity ratios less than one).

Therefore, the second phase of the program consisted of obtaining acoustic data from the same semi-annular nozzle configuration but, in this case, with velocity ratios of one or greater in order to eliminate the thrust loss penalty. The increased secondary stream exhaust velocity implies that, for the practical application, the secondary stream would have its own heat source. Precedents for this concept include the work on inverted velocity profile nozzles (refs. 3 and 4) and the coaxial nozzle annulus shaping results of references 5 and 6.

Acoustic data are presented for a 2.59 and 5.07 cm wide semi-annular secondary flow passage with a 10.0 cm diameter conical primary nozzle. Data are presented in the simulated flyover plane for locations on the same and

N84-13924#

opposite sides of the semi-annular secondary flow passage. Comparisons are also made between the experimental model results and predicted results for a fully-mixed conical nozzle alone.

Primary flow conditions varied from subsonic to supersonic (i.e., supercritical) over a range of total temperatures. Secondary flow was held at constant total temperature with total pressure varying so that velocity ratio (secondary to primary) varied from 1.0 to 1.4.

SYMBOLS

All dimensions in SI Units

D	diameter
h	annular gap width
M	Mach number
PNL	perceived noise level, PNdB
PR	nozzle pressure ratio
R	distance from center of nozzle exit plane to microphone
T	total temperature
V	velocity
w	weight flow rate
Δ PNL	change in perceived noise level
θ	directivity angle (measured from nozzle inlet centered on nozzle exit)
ϕ	azimuthal angle

Subscripts:

j	inner nozzle
s	outer nozzle

APPARATUS AND PROCEDURE

Facility

A photograph of the flow facility used for the acoustic experiments is shown in figure 1. A common unheated laboratory air source supplied flow for two parallel flow lines, one line for the inner nozzle and the other for the outer nozzle. Each flow line had its own air and fuel flow control and flow measuring systems. The air in each line could be heated by jet engine combustors. Mufflers in each line attenuated flow control valve noise and combustion noise. The system was designed for maximum nozzle exhaust

temperature of 1100 K and nozzle pressure ratios of 3.0 in both the inner and outer stream flow lines.

A sideline microphone array was used for the tests described herein. The microphones (0.635 cm) were placed at a constant 5.0 meter distance from and parallel to the nozzle axis, as shown in figure 2. The angles (θ) are based on the centerline of the nozzle exit plane. The microphones were located at positions corresponding to multiples of five degrees based on an assumed jet mixing noise distribution. The effective jet noise angles are also indicated in figure 2. The microphone grids were removed to improve high frequency performance. The ground plane of the test area was asphalt and concrete and covered with 15.25 cm thick foam rubber pads to help eliminate reflections.

Test Nozzles

A schematic of the test nozzle configurations is shown in figure 3. Existing coplanar coaxial nozzles (ref. 7) were modified to serve as the experimental models for the acoustic tests. The core or conical nozzle was common to both configurations and had an inner diameter of 10.00 cm. The small gap nozzle had a gap width of 2.59 cm and the large gap nozzle width was 5.07 cm. Two semi-circular steel rings were incorporated to block off one-half of the outer stream flow passage, as shown in the detail view in figure 3. The outer ring was fastened to the wall of the outer nozzle and the inner ring was fastened to the wall of the inner nozzle with a radial clearance between the two rings. This allowed unobstructed axial movement between the two flow lines as a result of differential thermal expansion. The outer wall of the inner nozzle was coated with a ceramic material to minimize heat transfer between the two streams during operation. The interior of the upstream portion of the inner nozzle supply line was also lined with insulating material.

Procedure

All tests were conducted with steady-state flow conditions for given nozzle total pressures and temperatures. Upstream plenum chamber total pressures and total temperatures were used to calculate nozzle exhaust velocities assuming ideal expansion to atmospheric conditions. Total temperatures were corrected for thermocouple radiation heat loss.

An on-line analysis of the noise signal from each microphone in succession was performed. One-third octave band sound pressure level spectra were digitally recorded and subsequently processed to give lossless data at the particular microphone location. Lossless data were obtained by adding atmospheric attenuation (ref. 8) to the spectral data. It was determined that the spectral data above 1000 Hz were free field (free from ground reflections) by comparing with the free field data reported in reference 7 for flow from the conic nozzle alone.

Perceived noise levels were calculated for a large scale nozzle by the method outlined in reference 9. The model data were scaled for size by a linear scale factor of 6.9 to give a 0.70 meter diameter for a representative engine size primary nozzle. Perceived noise levels were calculated at a

flyover distance of 335 meters for a standard day of 288 K and 70 percent relative humidity.

RESULTS AND DISCUSSION

Spectral comparisons are made here to show the effect of variation in velocity ratio between the two streams for two different azimuthal angles (ϕ). For simplicity, the nozzle will be stationary and the observer is assumed to be located either below the nozzle at $\phi = 0^\circ$, or above the nozzle at $\phi = 180^\circ$. At locations below the nozzle ($\phi = 0^\circ$) the secondary stream is between the primary stream and observer, and above the nozzle ($\phi = 180^\circ$) the secondary stream is on the side opposite the observer. Experimental data are then compared with predicted results for a conical nozzle alone operating at the same mixed flow properties as the two stream nozzle (same ideal thrust).

Effect of Velocity Ratio on Spectra

Spectral comparisons are shown for the 2.59 cm gap nozzle only, since trends for the 5.07 cm gap nozzle were similar. Spectral data below the nozzle at an azimuthal angle (ϕ) of zero degrees are shown in figure 4. Data are presented for three different directivity angles (θ) for a range of velocity ratios (V_s/V_j) at a constant subsonic primary nozzle flow condition.

At directivity angles of 46° (fig. 4(a)), and 95° (fig. 4(b)), the high frequency (>1000 Hz) sound pressure levels tend to increase with an increase in velocity ratio with the data for the higher velocity ratios (1.22 to 1.42) falling in a relatively narrow band. However, near the peak noise location at a directivity angle of 129° (fig. 4(c)), the effect of velocity ratio on high frequency sound pressure levels is greater than that at the forward angles.

Data above the nozzle at an azimuthal angle (ϕ) of 180° are shown in figure 5. The flow conditions are the same as in figure 4. Again, at a directivity angle of 46° (fig. 5(a)), and 95° (fig. 5(b)), the sound pressure levels tend to increase in the high frequency end of the spectrum with an increase in velocity ratio. For this case, however, in the rear quadrant at 129° (fig. 5(c)), the levels for all velocity ratios are practically the same up to 4 kHz. Above this frequency the levels for the low velocity ratio data ($V_s/V_j = 1.04$) begin to diverge while the higher velocity ratio data remain in good agreement.

A direct comparison of sound pressure level spectra below and above the nozzle for a velocity ratio of 1.04 and subsonic primary flow is shown in figure 6. At a directivity angle of 46° (fig. 6(a)), the sound pressure levels are essentially the same over the entire frequency range. At 95° (fig. 6(b)), the levels below the nozzle ($\phi = 0$) are slightly less than those above the nozzle for frequencies greater than 3150 Hz. In the rear quadrant at 129° (fig. 6(c)), the levels below the nozzle are, again, less than those above, but over a frequency range starting at about 630 Hz.

Sound pressure level comparisons at the two azimuthal locations for higher velocity ratios are shown in figure 7. Comparisons are shown only for a directivity angle of 129° , since at 46° and 95° the levels below and above the nozzle were practically identical for all velocity ratios. At a velocity ratio of 1.22 (fig. 7(a)), the sound pressure levels below the nozzle ($\phi = 0$) are slightly larger for frequencies greater than approximately 2000 Hz. As the velocity ratio is increased to 1.32 (fig. 7(b)), and then to 1.41 (fig. 7(c)), the high frequency (>1000 Hz) sound pressure levels below the nozzle become progressively greater than those above the nozzle. The levels above the nozzle ($\phi = 180^\circ$) are lower since the primary stream serves as a shield for the higher velocity secondary stream. These results are applicable only to the flyover plane since data for other azimuthal angles were not obtained.

Sound pressure level comparisons for supersonic primary flow are shown in figure 8. Again, only data for a directivity angle of 129° are shown since at 46° and 95° the difference in levels below and above the nozzle were minor. At a velocity ratio of 1.04 (fig. 8(a)), the sound pressure levels below the nozzle are less than those above. At a higher velocity ratio of 1.20 (fig. 8(b)), the trend is reversed with the levels below the nozzle being greater.

Perceived Noise Level Differences Below and Above Nozzle

The reduction of high frequency sound pressure levels for some cases shown in the previous section is an attractive consequence in terms of the reduction in perceived noise levels of large scale nozzles. This section presents the differences in perceived noise levels below and above the nozzle for various velocity ratios for a large scale single engine nozzle.

Flyover perceived noise level differences (ΔPNL) for the 2.59 cm gap nozzle for subsonic primary flow are shown in figure 9 as a function of distance along the flight path. The differences (ΔPNL) are equal to the perceived noise level above the nozzle ($\phi = 180^\circ$) minus the perceived noise level below the nozzle ($\phi = 0$). For a velocity ratio of 1.04 (fig. 9(a)), the perceived noise levels above the nozzle are greater than those below the nozzle for all points along the flight path. At the higher velocity ratios (figs. 9(b) to (d)), the perceived noise levels above the nozzle are less for distances greater than, at least, 270 meters behind the engine (-270 on the abscissa). For distances forward of this point the differences are essentially zero with an abrupt change occurring between -150 and -270 meters along the flight path.

Results for supersonic primary flow are shown in figure 10. Again, for a velocity ratio of 1.04 (fig. 10(a)), the levels above the nozzle are greater than those below. At a velocity ratio of 1.2 (fig. 10(b)), the effect is not large enough to show a consistent trend.

Perceived noise level differences for the 5.07 cm gap nozzle for subsonic primary flow are shown in figure 11. The trends are similar to those for the 2.59 cm gap nozzle. At a velocity ratio of 1.03 (fig. 11(a)), all perceived noise levels above the nozzle are greater than those below. At higher velocity ratios (figs. 11(b) to (d)), the levels above the nozzle are less for

distances greater than 270 meters behind the engine. Forward of this location the perceived noise levels above the nozzle are generally higher than those below.

Supersonic primary flow results for the 5.07 cm gap nozzle are shown in figure 12. At a velocity ratio of 1.03 (fig. 12(a)) the levels above the nozzle are greater except for large distances behind the engine (>400 meters). For the velocity ratio 1.22 case (fig. 12(b)), the levels above the nozzle are less for distances greater than 270 meters behind the engine. Forward of this location the perceived noise levels above the nozzle are greater than those below.

Comparison of Semi-Annular Nozzle Noise Data and Predicted Results for a Mixed-Flow Conical Nozzle

Predicted mixed-flow conical nozzle noise results were evaluated by the method outlined in reference 10. Temperature and velocity of the exhaust stream of the conical nozzle were the same as the weight averaged temperature and velocity calculated for the semi-annular configuration. Comparisons made on this basis assure that the two nozzle configurations have the same ideal thrust for the same total weight flow.

Sound pressure level below and above the semi-annular nozzle are compared with predicted results for a mixed-flow conical nozzle in figure 13. Data are shown for three different directivity angles for subsonic primary flow from the 2.59 cm gap semi-annular configuration. Velocity ratio for the semi-annular nozzle is 1.32 but the trends shown are representative for other velocity ratios. Flow from the conical nozzle alone is slightly supersonic. At a directivity angle of 46° (fig. 13(a)), the data and predicted results fall in a narrow band over the entire frequency range. At 95° (fig. 13(b)), again, the data and prediction agree fairly well up to about 8 kHz and then the sound pressure levels for the conical nozzle become less than those for the semi-annular configuration. At 129° (fig. 13(c)), the predicted results for the conical nozzle agree fairly well with the data above the semi-annular nozzle ($\phi = 180^\circ$) up to a frequency at approximately 8 kHz and then the predicted levels diverge from the data. Below the semi-annular nozzle ($\phi = 0^\circ$), the levels are significantly above those of the mixed-flow conical nozzle.

A comparison of data for supersonic primary flow from the semi-annular nozzle for a velocity ratio of 1.04 and predicted conical nozzle results is shown in figure 14. At 46° (fig. 14(a)), the data above the semi-annular nozzle agree closely with the prediction. Conversely, at 95° (fig. 14(b)), and 129° (fig. 14(c)), the data below the semi-annular nozzle ($\phi = 0^\circ$) are in closer agreement with the prediction, while above the semi-annular nozzle the levels are above the mixed-flow conical nozzle prediction.

Data for a 1.2 velocity ratio case and supersonic primary semi-annular nozzle flow are compared with the conical nozzle alone prediction in figure 15. At 46° (fig. 15(a)), the prediction shows a large shock noise component peaking at 2500 Hz considerably above the data for the semi-annular nozzle. At 95° (fig. 15(b)), the data and prediction are in close agreement over the frequency range shown. In the rear quadrant at 129° (fig. 15(c)), the data

above the semi-annular nozzle agrees with the levels predicted for the conical nozzle, while the levels below the nozzle are somewhat higher. Similar results were obtained for the 5.07 cm gap semi-annular nozzle.

The above results indicate the semi-annular configuration offers very little, if any, noise reduction benefits compared to noise levels for a mixed-flow conical nozzle.

CONCLUSIONS

An experiment was conducted to determine the noise generating characteristics of a conical nozzle with a semi-annular flow passage having secondary to primary velocity ratios ranging from 1.0 to 1.4. Spectral data are presented at different directivity angles in the flyover plane with the semi-annular flow passage located either on the same side or opposite side relative to an observer. Comparisons are also made with predicted noise levels for a mixed-flow conical nozzle. The results of the tests may be summarized as follows:

(1) The combination of the conical nozzle and semi-annular flow passage shows no improvement in terms of noise reduction when compared to predicted results from a mixed-flow conical nozzle operating at the same total thrust.

(2) For the 2.59 cm wide annular gap nozzle, at velocity ratios greater than 1.0 and subsonic primary flow, peak perceived noise levels in the rear quadrant were reduced by about 5 PNdB by placing the secondary passage on the side opposite an observer. At forward locations different orientations of the passage had essentially no effect. For supersonic primary flow and velocity ratios greater than 1.0 orientation of the secondary flow passage had little effect on perceived noise levels.

(3) For the 5.07 cm wide annulus and velocity ratios greater than 1.0, perceived noise levels were greater in the forward quadrant and less in the aft quadrant when the secondary passage was on the side opposite an observer. This was true for either subsonic or supersonic primary flow.

REFERENCES

1. Goodykoontz, J. H.: Effect of Semi-Annular Thermal Acoustic Shield on Jet Exhaust Noise. NASA TM-81615, 1980.
2. Goodykoontz, J. H.: Fluid Shielding of High Velocity Jet Noise. NASA TP- , 1983.
3. Knott, P. R.; and et al.: Acoustic Tests of Duct-Burning Turbofan Jet Noise Simulation. (R77AEG524, General Electric Co.; NASA Contract NAS3-18008.) NASA CR-2966, 1978.
4. Kozlowski, H.; and Packman, A. B.: Aerodynamic and Acoustic Tests of Duct-Burning Turbofan Exhaust Nozzles. (PWA5296, Pratt and Whitney Aircraft; NASA Contract NAS3-17866.) NASA CR-2628, 1976.
5. von Glahn, U.; and Goodykoontz, J. H.: Noise Suppression Due to Annulus Shaping of a Conventional Coaxial Nozzle. NASA TM-81461, 1980.
6. Goodykoontz, J. H.; and von Glahn, U.: Noise Suppression Due to Annulus Shaping of an Inverted-Velocity-Profile Coaxial Nozzle - Supersonic Cruise Aircraft, NASA TM-81460, 1980.

7. Goodykoontz, J. H.; and Stone, J. R.: Experimental Study of Coaxial Nozzle Exhaust. AIAA Paper No. 79-0631, March 1979.
8. Shields, F. D.; and Bass, H. E.: Atmospheric Absorption of High Frequency Noise and Application to Fractional-Octave Bands. (Mississippi Univ.; NASA Contract NAS3-19431.) NASA CR-2760, 1977.
9. Definitions and Procedures for Computing the Perceived Noise Level of Aircraft Noise. Aerospace Recommended Practice 865A, Aug. 1969, SAE.
10. Stone, J. R.; Groesbeck, D. E.; and Zola, C. L.: Conventional Profile Coaxial Jet Noise Prediction. AIAA J., vol. 21, no. 3, Mar. 1983, pp. 336-342.

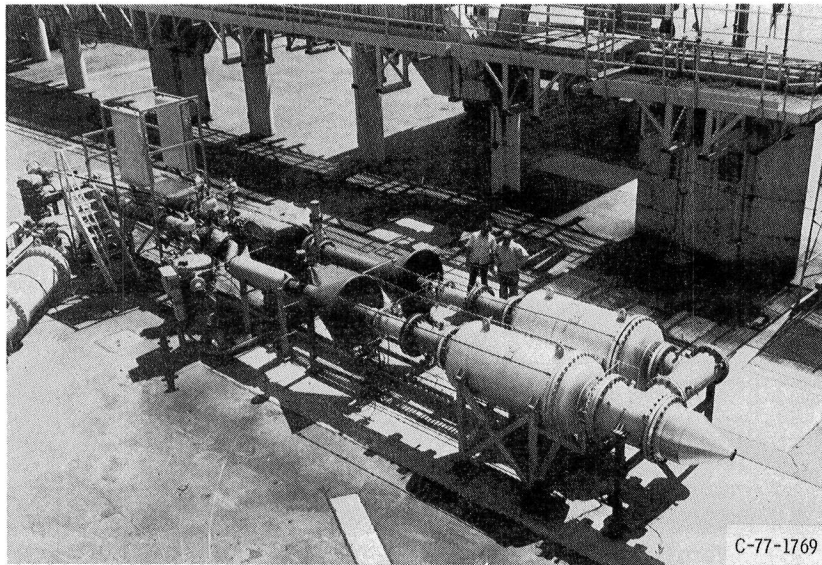


Figure 1. - Lewis hot jet acoustic facility.

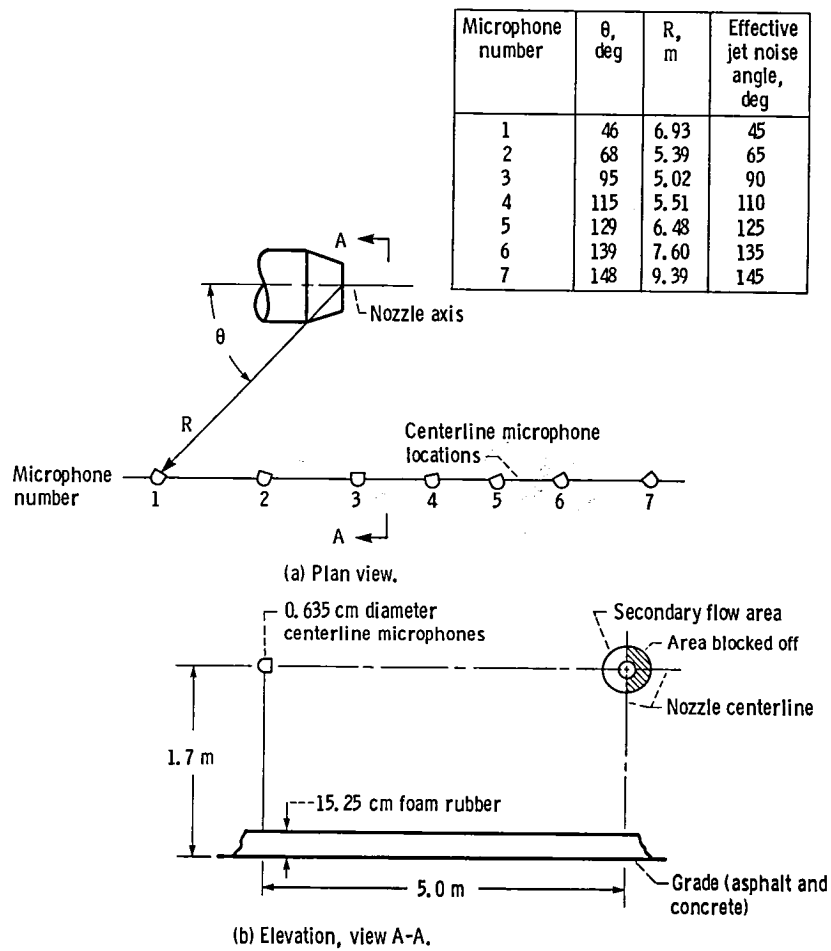


Figure 2. Schematic of flyover microphone layout.

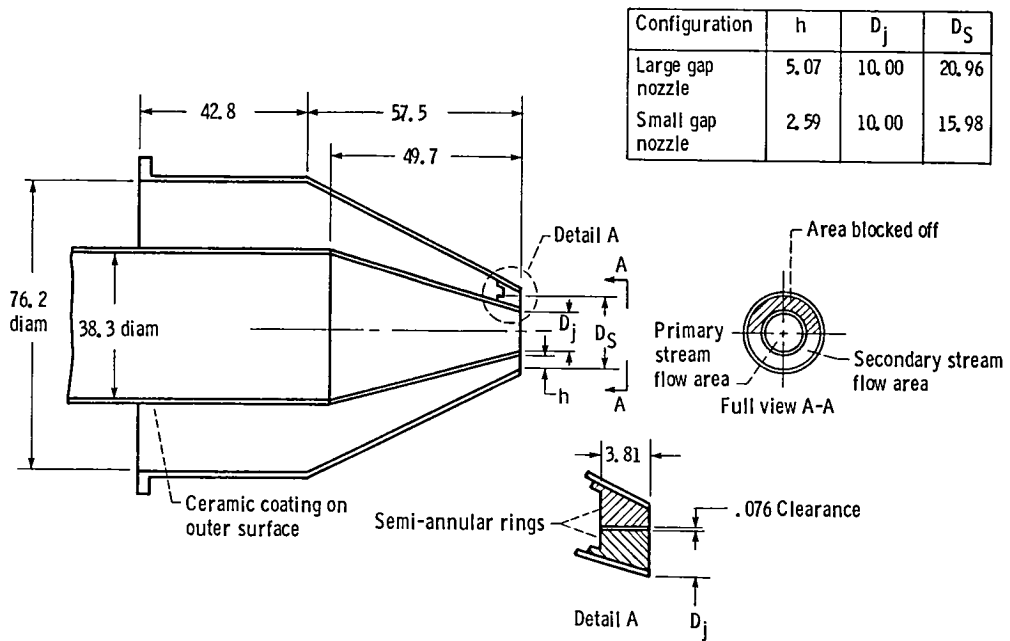


Figure 3. - Schematic of nozzle configurations. All dimensions in centimeters.

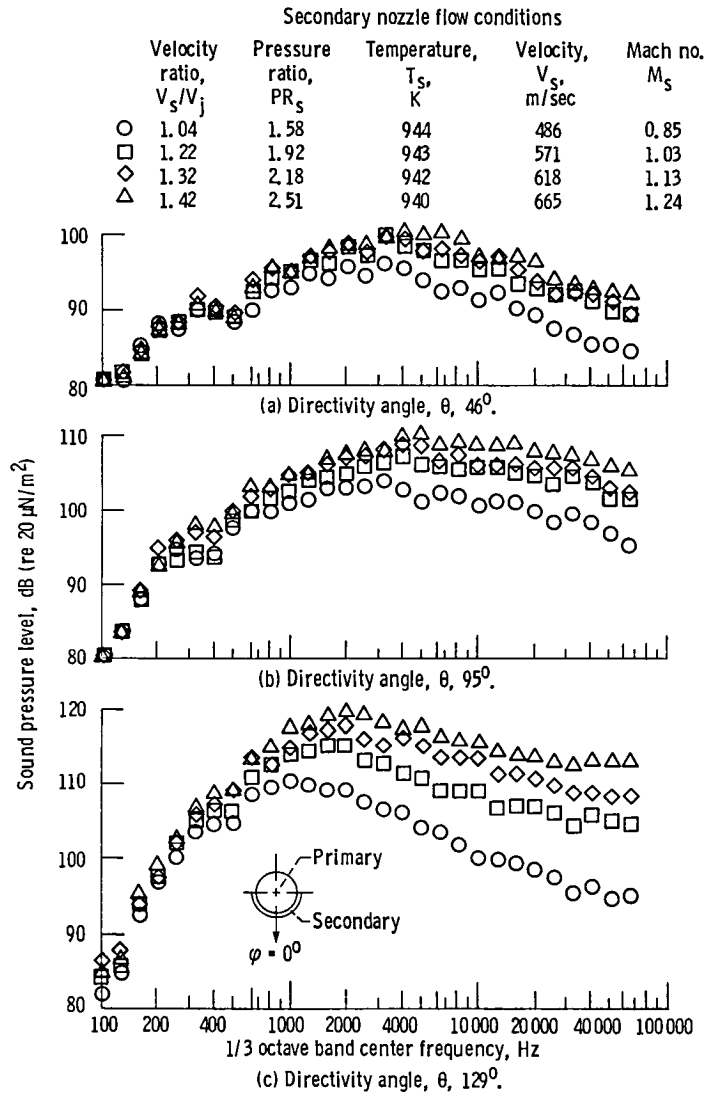


Figure 4 - Effect of velocity ratio on sound pressure levels for the 2.59 cm gap nozzle at an azimuthal angle of zero degrees and subsonic primary nozzle flow. Primary nozzle nominal flow conditions; $PR_j = 1.8$, $T_j = 696$ K, $V_j = 469$ m/sec, $M_j = 0.97$.

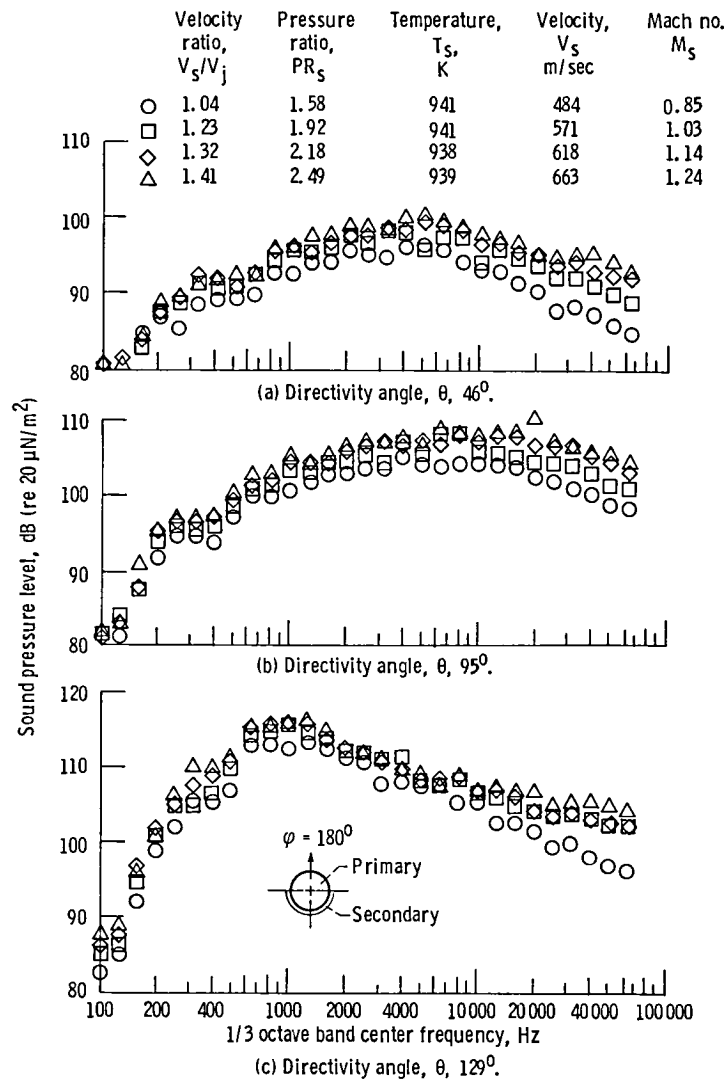


Figure 5. - Effect of velocity ratio on sound pressure levels for the 2.59 cm gap nozzle at an azimuthal angle of 180 degrees and subsonic primary nozzle flow. Primary nozzle nominal flow conditions: $PR_j = 1.80$, $T_j = 694$ K, $V_j = 466$ m/sec, $M_j = 0.97$.

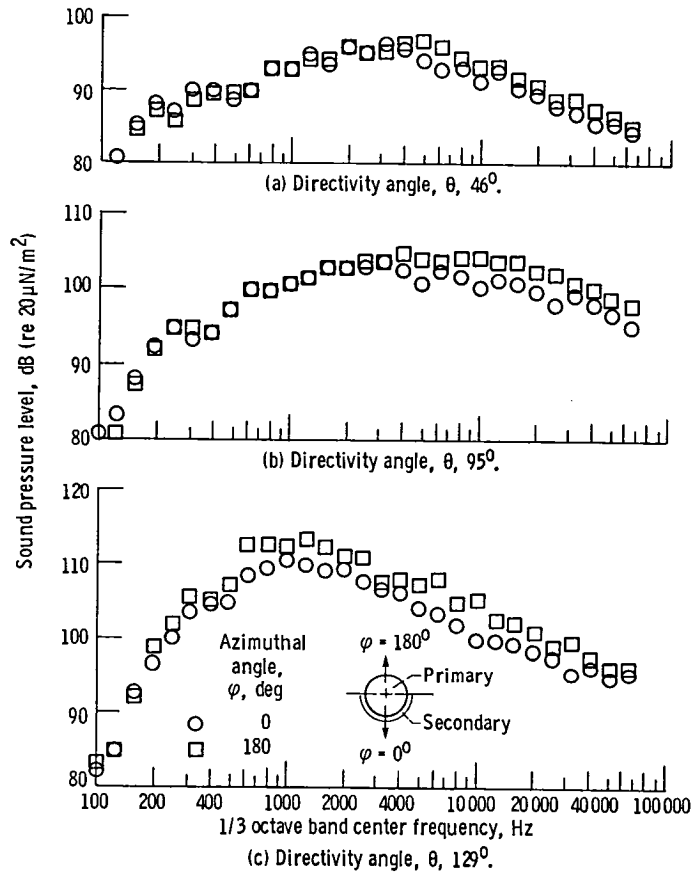


Figure 6. - Comparison of sound pressure levels below and above 2.59 cm gap nozzle for velocity ratio of 1.04 and subsonic primary nozzle flow, Nominal flow conditions: $PR_i = 1.8$, $T_i = 696$ K, $V_i = 469$ m/sec, $M_i = 0.97$; $PR_s = 1.58$, $T_s = 944$ K, $V_s = 486$ m/sec, $M_s = .85$.

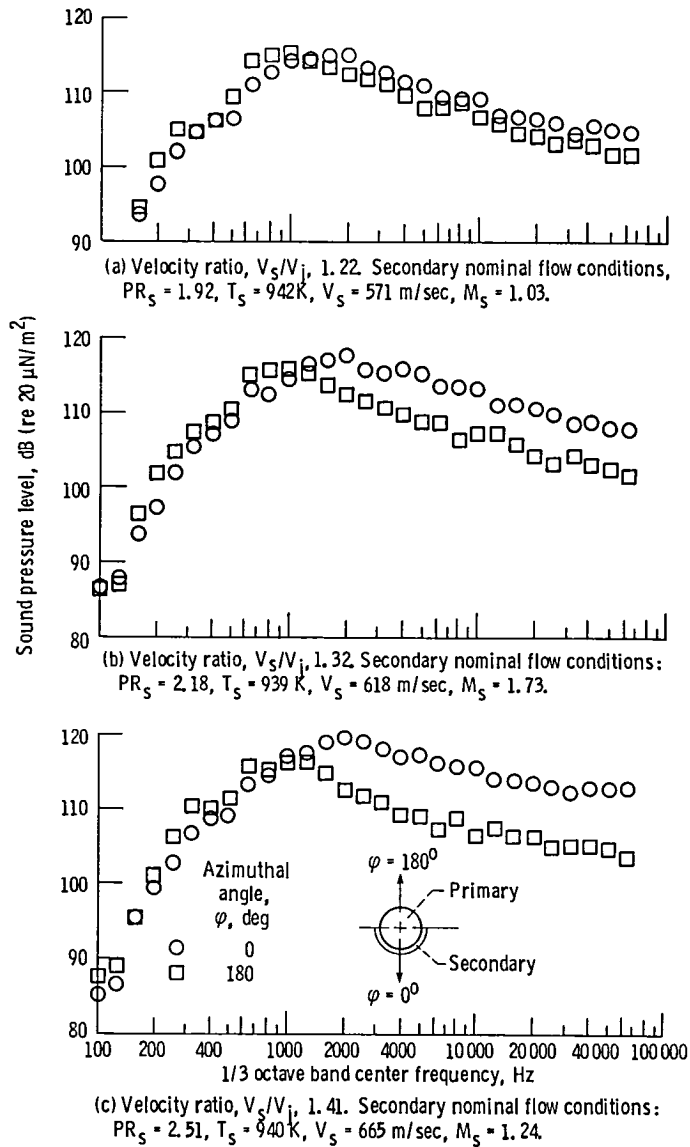


Figure 7. - Comparison of sound pressure levels below and above 2.59 cm gap nozzle for various velocity ratios and subsonic primary flow. Directivity angle, θ , 129 degrees. Primary nominal flow conditions: $PR_j = 1.80$, $T_j = 695\text{ K}$, $V_j = 468\text{ m/sec}$, $M_j = .97$.

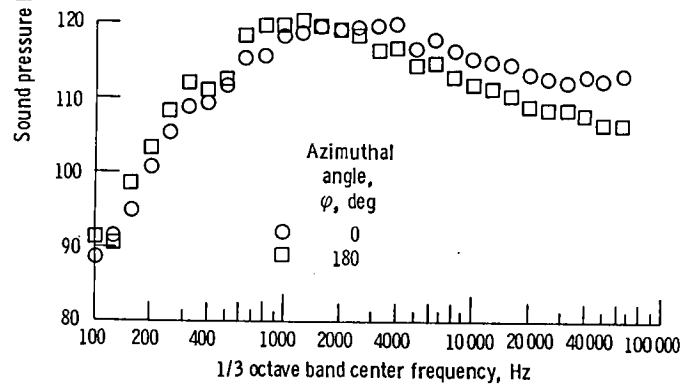
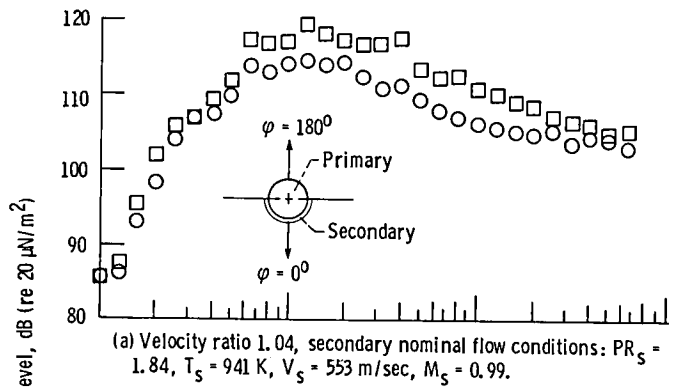


Figure 8. - Comparison of sound pressure levels below and above 2.59 cm gap nozzle for various velocity ratios and supersonic primary nozzle flow. Directivity angle, θ , 129° . Primary nominal flow conditions: $PR_j = 2.20$, $T_j = 694$ K, $V_j = 534$ m/sec, $M_j = 1.14$

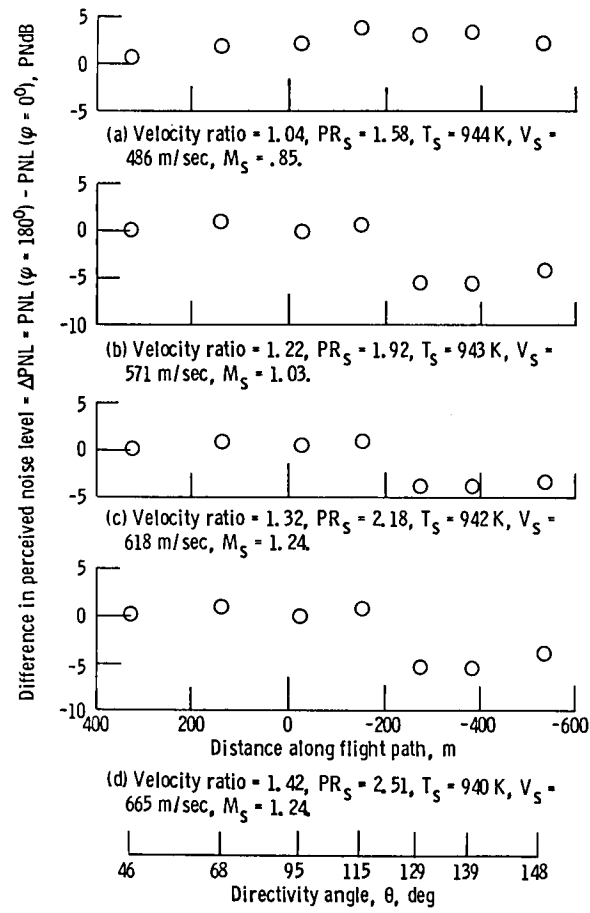


Figure 9. - Differences in flyover perceived noise levels below and above 2.59 gap nozzle scaled to full size. Subsonic primary flow: $PR_j = 1.8$, $T_j = 696$ K, $V_j = 469$ m/sec, $M_j = 0.97$

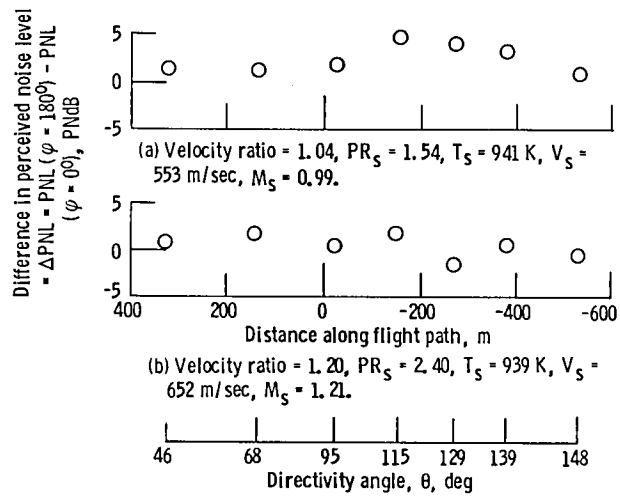


Figure 10. - Differences in flyover perceived noise levels below and above 2.59 gap nozzle scaled to full size. Supersonic primary flow: $PR_j = 2.20$, $T_j = 694$ K, $V_j = 534$ m/sec, $M_j = 1.14$.

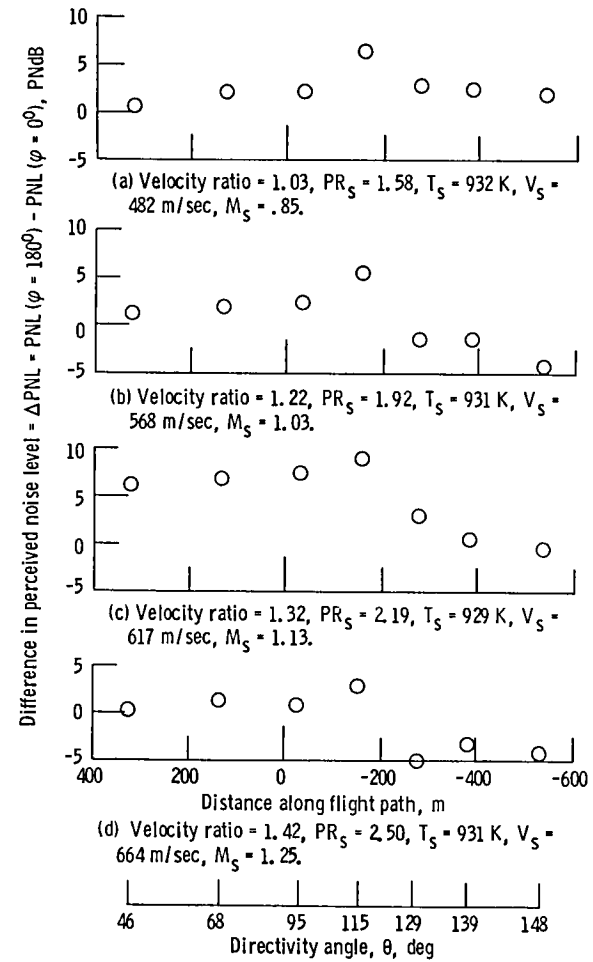


Figure 11. - Differences in flyover perceived noise levels below and above 5.07 cm gap nozzle scaled to full size. Subsonic primary flow: $PR_j = 1.81$, $T_j = 696$ K, $V_j = 469$ m/sec, $M_j = 0.97$.

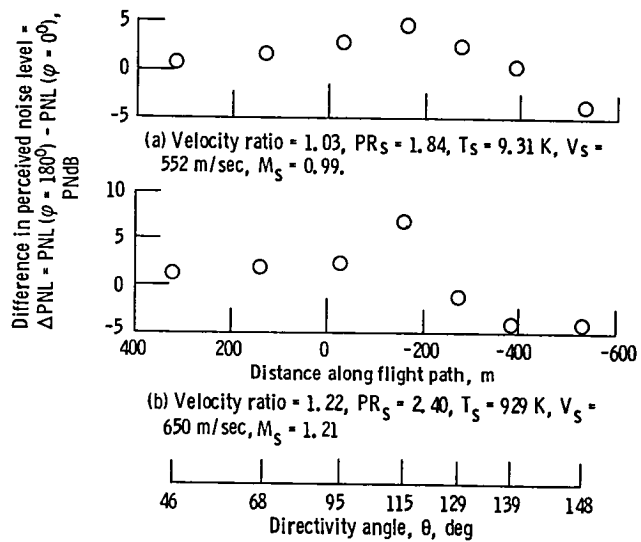


Figure 12 - Differences in flyover perceived noise levels below and above 5.07 cm gap nozzle scaled to full size. Supersonic primary flow: $\text{PR}_j = 2.23$, $T_j = 693 \text{ K}$, $V_j = 538 \text{ m/sec}$, $M_j = 1.14$.

	Nozzle flow conditions									
	PR _j	T _j , K	V _j , m/sec	M _j	W _j , kg/sec	PR _s	T _s , K	V _s , m/sec	M _s	W _s , kg/sec
Semi-annular nozzle	1.81	693	467	0.97	2.02	2.18	939	618	1.13	1.45
Conical nozzle prediction Diameter = 12.28 cm	1.96	800	532	1.04	3.47					

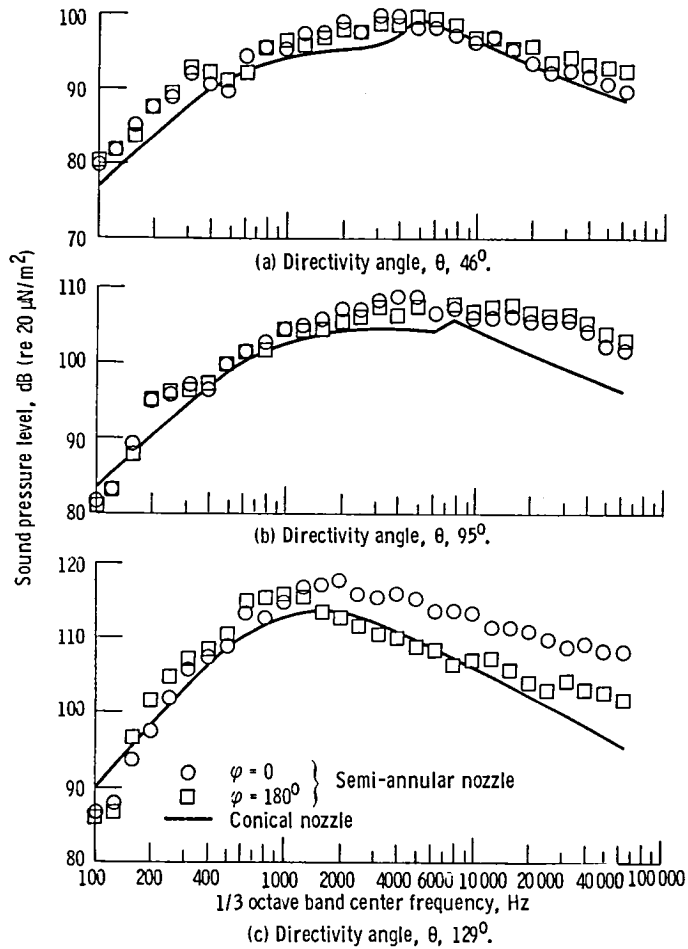


Figure 13. - Comparison of subsonic primary semi-annular nozzle data with predicted conical nozzle alone results. Semi-annular nozzle velocity ratio 1.32. Same ideal thrust for both nozzle configurations.

	Nozzle flow conditions									
	PR _j	T _j , K	V _j , m/sec	M _j	W _j , kg/sec	PR _s	T _s , K	V _s , m/sec	M _s	W _s , kg/sec
Semi-annular nozzle	2.20	694	534	1.14	2.52	1.84	941	553	.99	1.20
Conical nozzle prediction Diameter = 12.12 cm	2.05	775	5.41	1.08	3.70					

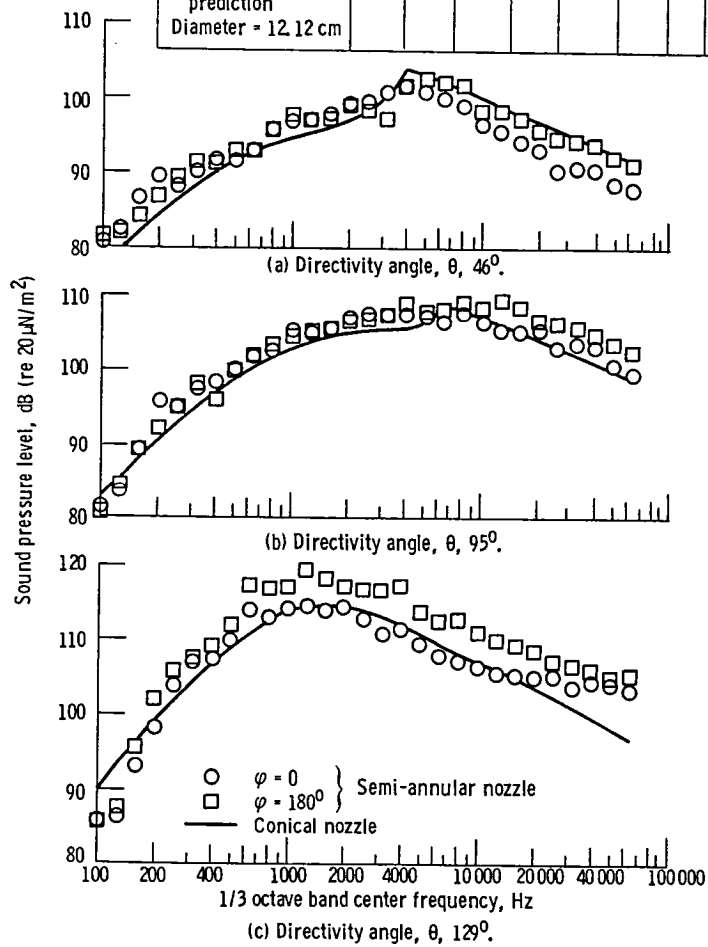


Figure 14 - Comparison of supersonic primary semi-annular nozzle data with predicted conical nozzle results. Semi-annular nozzle velocity ratio 1.03. Same ideal thrust for both nozzle configurations.

	Nozzle flow conditions									
	PR _j	T _j , K	V _j , m/sec	M _j	W _j , kg/sec	PR _s	T _s , K	V _s , m/sec	M _s	W _s , kg/sec
Semi-annular nozzle	2.20	696	535	1.14	2.51	2.40	030	652	1.21	1.61
Conical nozzle prediction Diameter = 11.68 cm	2.27	792	581	1.17	4.12					

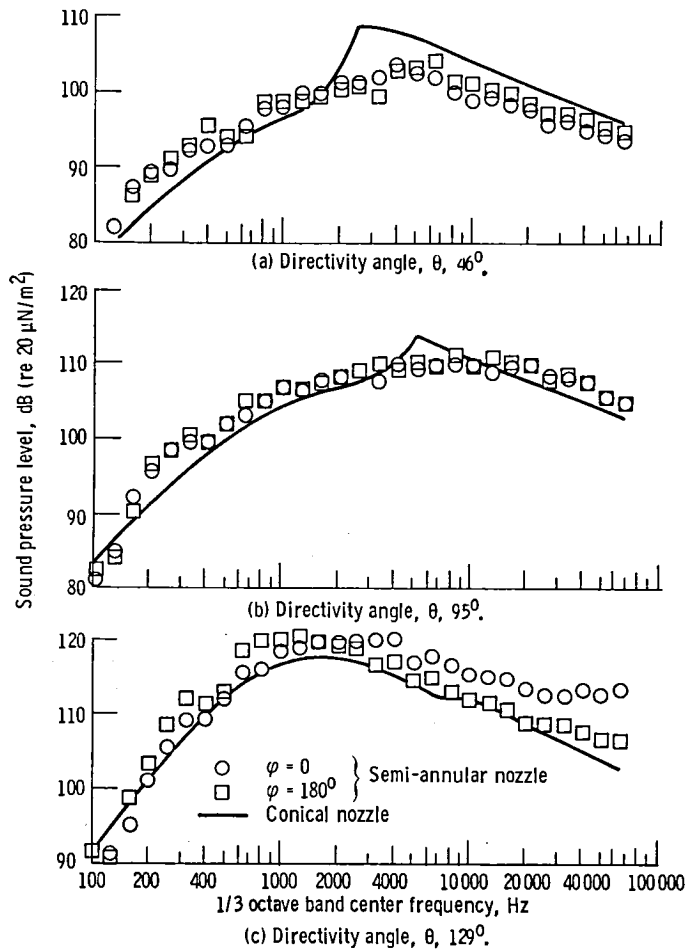
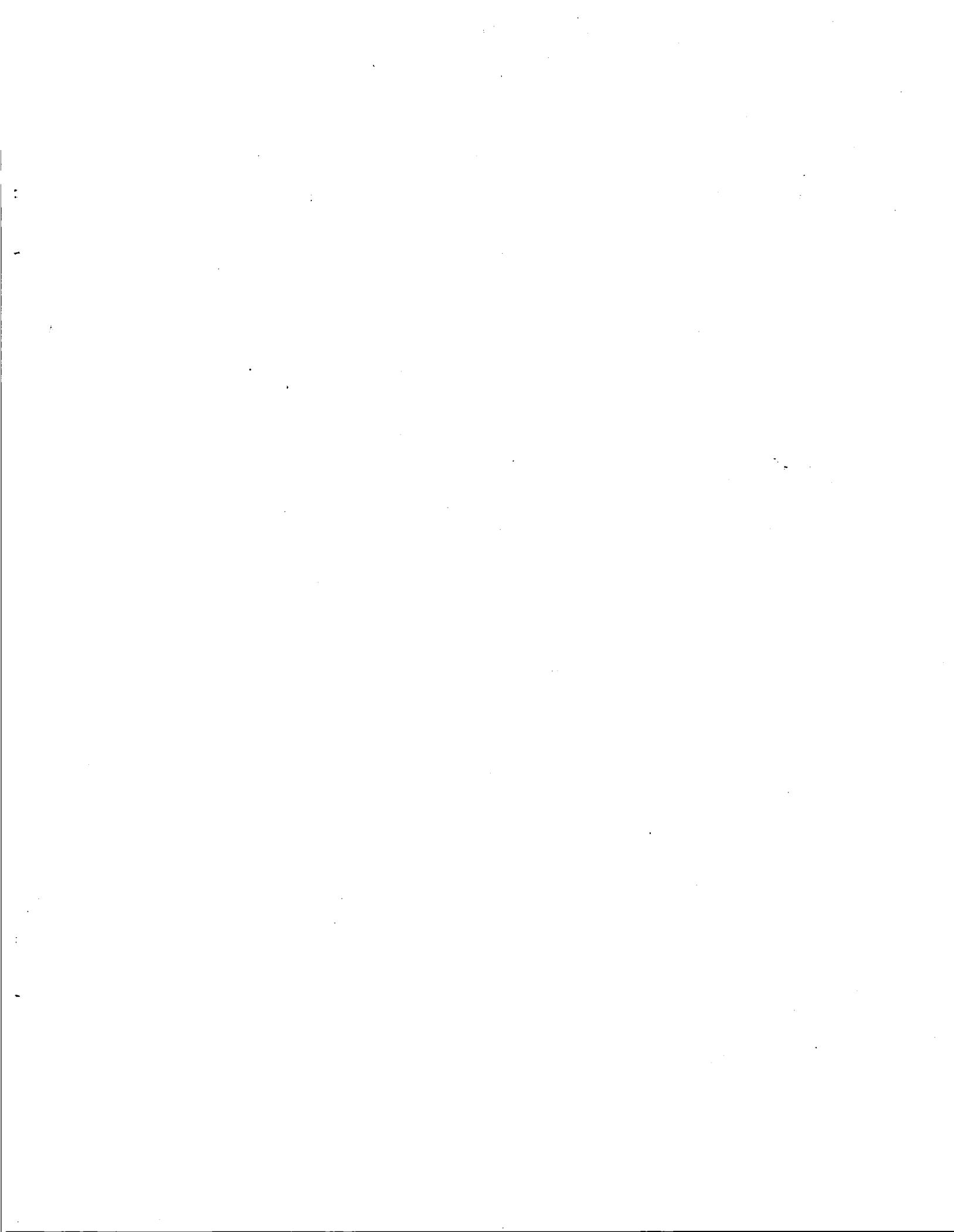


Figure 15. - Comparison of supersonic primary semi-annular nozzle data with predicted conical nozzle alone results. Semi-annular nozzle velocity ratio 1.22. Same ideal thrust for both nozzle configurations.

1. Report No. NASA TM-83525		2. Government Accession No.		3. Recipient's Catalog No.	
4. Title and Subtitle Inverted Velocity Profile Semi-Annular Nozzle Jet Exhaust Noise Experiments				5. Report Date December 1983	
				6. Performing Organization Code 505-31-32	
7. Author(s) Jack H. Goodykoontz				8. Performing Organization Report No. E-1890	
				10. Work Unit No.	
9. Performing Organization Name and Address National Aeronautics and Space Administration Lewis Research Center Cleveland, Ohio 44135				11. Contract or Grant No.	
				13. Type of Report and Period Covered Technical Memorandum	
12. Sponsoring Agency Name and Address National Aeronautics and Space Administration Washington, D.C. 20546				14. Sponsoring Agency Code	
15. Supplementary Notes					
16. Abstract Experimental noise data are shown for a conical nozzle with a semi-annular secondary flow passage having secondary to primary velocity ratios ranging from 1.0 to 1.4. Spectral data are presented at different directivity angles in the flyover plane with the semi-annular flow passage located either on the same side or opposite side relative to an observer. A 10.0 cm diameter primary conical nozzle was used with a 2.59 cm and 5.07 cm wide annular gap secondary nozzle. Similar trends were observed for both nozzle configurations. In general, near the peak noise location and at velocity ratios greater than 1.0, noise levels were larger on the side where the secondary passage was closest to an observer. At velocity ratios near 1.0 the opposite was true. When compared to predicted noise levels for a conical nozzle alone operating at the same ideal thrust, the semi-annular configuration showed no benefit in terms of noise attenuation.					
17. Key Words (Suggested by Author(s)) Jet noise; Jet shielding; Inverted velocity profile nozzles				18. Distribution Statement Unclassified - unlimited STAR Category 71	
19. Security Classif. (of this report) Unclassified		20. Security Classif. (of this page) Unclassified		21. No. of pages	22. Price*



National Aeronautics and
Space Administration

Washington, D.C.
20546

Official Business
Penalty for Private Use, \$300

SPECIAL FOURTH CLASS MAIL
BOOK



Postage and Fees Paid
National Aeronautics and
Space Administration
NASA-451

NASA

POSTMASTER: If Undeliverable (Section 158
Postal Manual) Do Not Return
